A&A, 709, L14 (2026)
https://doi.org/10.1051/0004-6361/202659044

Astronomy & Astrophysics

LETTER TO THE EDITOR

First measurement of the Hubble constant from a combined weak-lensing and gravitational-wave standard siren analysis

Felipe Andrade-Oliveira*, David Sanchez-Cid, Danny Laghi, and Marcelle Soares-Santos

Physik-Institut, Universität Zürich, Winterthurerstrasse 190, 8057 Zürich, Switzerland

Received 19 January 2026 / Accepted 16 March 2026

ABSTRACT

We present a new measurement of the Hubble constant (H_0) resulting from the first joint analysis of standard sirens with weak gravitational lensing and galaxy clustering observables comprising three two-point correlation functions (3×2 pt). For the 3×2 pt component of the analysis, we used data from the Dark Energy Survey (DES) Year 3 release. For the standard siren component, we used data from the Gravitational-Wave Transient Catalog 4.0 released by the LIGO-Virgo-KAGRA (LVK) Collaboration. For GW170817, the only standard siren for which extensive electromagnetic follow-up observations exist, we also used measurements of the host galaxy redshift and inclination angle estimates derived from observations of a superluminal jet from its remnant. Assuming a flat Λ cold dark matter model, our joint analysis yields $H_0 = 67.94^{+4.40}_{-4.34}$ km s^{-1} Mpc^{-1}, a 6.4% measurement, while improving the DES constraint on the total abundance of matter Ω_m by 22%. When the jet information is removed, the H_0 precision decreases to 9.9%. The measurement of H_0 remains a central problem in cosmology, with a multitude of approaches being vigorously pursued with the aim to reconcile significantly discrepant measurements at the percent level. In light of the impending new data releases from DES and LVK, and anticipating a much higher constraining power from 3×2 pt observables using newly commissioned survey instruments, we demonstrate that incorporating standard sirens in the cosmology framework of large cosmic surveys is a viable route towards that goal.

Key words. gravitational lensing: weak – gravitational waves – cosmological parameters – large-scale structure of Universe

1. Introduction

The measurement of the present-day expansion rate, the Hubble constant (H_0), poses an empirical challenge to the ΛCDM cosmological model. H_0 values inferred from the early Universe through analyses of the cosmic microwave background (CMB) data under the ΛCDM assumption (Planck Collaboration VI 2020; Louis et al. 2025; Camphuis et al. 2026) are in significant ($\gtrsim5\sigma$) tension, with direct measurements obtained from late-Universe observables such as type Ia supernovae (SNe Ia) calibrated using the cosmic distance ladder (Riess et al. 2022). While many analyses of the early- (Efstathiou & Gratton 2021; Hou et al. 2018) and late-time (Casertano et al. 2025; Di Valentino & Brout 2024) sides have been carried out to reconcile these measurements, the problem persists.

Motivated by this scenario, we present a new measurement of the Hubble constant resulting from an independent analysis of multi-messenger observables. Our approach builds upon the well-established multi-probe framework, known as the 3×2 pt analysis in the photometric survey community (Abbott et al. 2022; Heymans et al. 2021; Miyatake et al. 2023). This framework combines the weak -lensing cosmic shear 2-point correlation function (2PCF) (Secco et al. 2022; Amon et al. 2022; Wright et al. 2025), which is sensitive to the sum of baryonic and dark matter abundance (Ω_m) and the amplitude of matter density fluctuations, with galaxy clustering 2PCF (Rodríguez-Monroy et al. 2022) and the cross-correlation of galaxy shear and position fields (Prat et al. 2022; Pandey et al. 2022; Porredon et al. 2022). We added gravitational wave (GW) distance indicators known as standard sirens (Holz & Hughes 2005) to the 3×2 pt observables. These distance indicators are binary coalescence events that are used for ΛCDM cosmological measurements (Abac et al. 2025a) with redshift information gathered from electromagnetic (EM) counterpart observations (Abbott et al. 2017a), catalogues of likely host galaxies (Soares-Santos et al. 2019; Abbott et al. 2021; Finke et al. 2021; Palmese et al. 2023; Mastrogiovanni et al. 2023; Bom et al. 2024; Mukherjee et al. 2024; de Matos et al. 2025), and the mass spectrum of the binary population (Taylor et al. 2012; Ezquiaga & Holz 2022; Abbott et al. 2023; Karathanasis et al. 2023). We also used information from follow-up observations of the EM counterpart of the standard siren GW170817 (Abbott et al. 2017b,c; Mooley et al. 2018) that enhance its constraining power for cosmology (Hotokezaka et al. 2019). As neither standard sirens nor the 3×2 pt observables rely on the cosmic distance ladder, this work shows that incorporating gravitational waves into the multi-probe cosmology framework of large surveys is a viable route to constrain H_0 and thereby inform the ongoing debate.

2. Data

The DES is a *grizY* photometric survey that mapped 5000 deg^2 of the southern sky from Cerro Tololo, Chile, using the Dark Energy Camera (DECam; Flaugher et al. 2015) between 2013 and 2019. The DES Y3 data release includes the first three years (Sevilla-Noarbe et al. 2021). We used the data vectors published in Abbott et al. (2022)[1]. The weak-lensing signal was extracted from a source galaxy sample drawn from a galaxy shape catalogue (Gatti et al. 2021) comprising about 100 million

* Corresponding author:
felipe.andradeoliveira@physik.uzh.ch

[1] https://des.ncsa.illinois.edu/releases/y3a2/Y3key-products

galaxies, divided into four tomographic redshift bins up to $z = 2$, effective source density of $n_{\rm eff} = 5.9$ galaxies per arcmin^2 and a shape noise of $\sigma_{\rm e} = 0.26$. Galaxy clustering was measured using the MAGLIM lens galaxy sample (Porredon et al. 2021, 2022), which contains 10.7 million galaxies split into six redshift bins. Redshift distributions for the source and lens samples were derived using self-organising maps (Giannini et al. 2024) and the directional neighbourhood fitting method (De Vicente et al. 2016), respectively.

The LIGO-Virgo-KAGRA Collaboration (LVK) network of observatories (Abac et al. 2025b) consists of two Laser Interferometer Gravitational-Wave Observatory (LIGO; Aasi et al. 2015) detectors in the USA plus Virgo (Acernese et al. 2015) in Europe and KAGRA (Akutsu et al. 2021) in Japan. These four detectors are enhanced Michelson interferometers sensitive to gravitational waves in the ∼10–1000 Hz band (Abac et al. 2025b). The LVK realises observing runs in which one or more detectors are operational. The fourth Gravitational-Wave Transient Catalog (GWTC-4.0; Abac et al. 2025b,c,d) comprises GW transient candidates accumulated between the first observing run (O1) and the end of the first part of the fourth observing run (O4a), which ended in January 2024. The catalogue reports the inferred source parameters under the hypothesis that these transients are caused by GWs emitted by compact binary coalescence (CBCs). This catalogue has been used to study the population properties of CBCs (Abac et al. 2025e) and to constrain late-time cosmological parameters (Abac et al. 2025a). We used the data presented in Abac et al. (2025a)[2]. We took the posterior samples for H_0 and Ω_m obtained using 142 CBCs out of the 218 GW candidates included in GWTC-4.0. We specifically chose the subset of the posteriors corresponding to the spectral sirens analysis, which exclusively relies on the GW data. GW170817 (Abbott et al. 2017b,c) is the only GWTC-4.0 bright siren (i.e. a CBC with a confirmed EM counterpart). To re-analyse GW170817 for this work, we also used the injection files (Essick et al. 2025; Abac et al. 2025c) that were used to correct for GW selection effects and the posterior samples for all its CBC parameters, including the luminosity distance (d_L) and the source inclination angle (θ_{JN}).

The discovery of its EM counterpart (Abbott et al. 2017c) means that a wealth of multi-messenger data on GW170817 is available. This allowed us to supplement the GW data with information derived from follow-up observations of the counterpart itself, as well as with archival data such as the spectroscopic redshift of the host galaxy, NGC 4993, and the velocity field at its position. We used the host recession velocity $v = 3327 \pm 72\,{\rm km\,s^{-1}}$ (Crook et al. 2007) relative to the CMB and the radial peculiar velocity $\langle v_p \rangle = 310 \pm 150\,{\rm km\,s^{-1}}$ (Carrick et al. 2015). We also used the inclination angle constraint, $15^\circ < \theta_{\rm jet} < 29^\circ$, obtained from observations of superluminal motion of the remnant jet between 75 and 230 days post-merger (Mooley et al. 2018; Hotokezaka et al. 2019).

3. Methods

In the 3×2 pt framework, cosmological information is inferred from overdensity and shear fields constructed from observations of galaxy positions and shapes. Field-level information is then compressed into the three 2PCFs shear-shear, galaxy-galaxy, and galaxy-shear, which in turn can be jointly compared to the cosmological model predictions (Krause et al. 2021; Friedrich et al. 2021). The theoretical framework is complemented with the modelling of known astrophysical and calibration systematic effects, such as galaxy bias (Porredon et al. 2022), intrinsic alignment (Blazek et al. 2019), lens magnification (Elvin-Poole et al. 2023), and redshift and galaxy shape calibration (Cawthon et al. 2022; Giannini et al. 2024; MacCrann et al. 2021). It also includes an analytical estimate of the signal covariance (Krause & Eifler 2017; Fang et al. 2020).

We used the spectral siren results from Abac et al. (2025a). We summarise their approach. The GW waveform produced by a CBC with intrinsic mass M at redshift z is the same as that from an otherwise equivalent system of intrinsic mass $(1+z)M$ at redshift zero. This degeneracy between source-frame mass and redshift prevents us from directly obtaining the source redshift from the parameter estimation (PE) of a CBC transient. However, redshift information can be obtained through the general framework of Bayesian hierarchical inference (Mandel et al. 2019; Vitale et al. 2022). This framework assumes that single-event CBC parameters are drawn from a population distribution. This distribution is described by a set of parameters that are inferred jointly with the cosmological parameters of interest and later marginalised over as nuisance parameters.

To obtain multi-messenger cosmological posterior samples for GW170817, we started with the GW-only PE samples from the LVK analysis in Abbott et al. (2019) and incorporated the inclination angle information from Mooley et al. (2018) by running an importance sampling algorithm using the EM-derived θ_{JN} range as an external flat prior. This procedure is similar to the one followed by Hotokezaka et al. (2019) and assumes that the jet emission is perpendicular to the orbital plane. The estimated θ_{JN} range is weakly dependent on d_L. We tested the effect of this dependence in our analysis and found it to be negligible.

To achieve our multi-messenger cosmology results, we combined the DES Y3 3×2 pt observables with 142 LVK standard sirens (141 spectral sirens plus GW170817). In practice, we combined posterior distributions, assuming they are independent. The choice to use LVK posterior samples from the spectral sirens method instead of the dark sirens method, which constructs line-of-sight redshift priors from a galaxy catalogue, avoids systematic uncertainties arising from covariances between the two types of probes, which would use overlapping galaxy catalogues. The loss of constraining power due to this choice is modest, as spectral sirens are much more constraining than dark sirens in the GWTC-4.0 LVK cosmology analysis (Abac et al. 2025a). In the 3×2 pt and the standard siren cases, we inferred the cosmological parameters $\mathbf{s}_{\rm c} = \{H_0, \Omega_m\}$ while marginalising over a set of nuisance parameters $\mathbf{s}_{\rm n}$, which may include other cosmological parameters and astrophysical or calibration parameters. We adopted $H_0 \in [10, 200]\,{\rm km\,s^{-1}\,Mpc^{-1}}$ and $\Omega_m \in [0, 1]$ as priors.

For the 3×2 pt analysis, we assumed a Gaussian likelihood,

$$\mathcal{L}\left(\mathbf{D} \,\middle|\, \mathbf{s}_{\rm c}, \mathbf{s}_n\right) \propto \exp\left\{-\frac{1}{2}\mathbf{R}^{\intercal}{\rm Cov}^{-1}\mathbf{R}\right\}, \tag{1}$$

with the column matrix $\mathbf{R} = \mathbf{D} - \mathbf{T}(\mathbf{s}_{\rm c}, \mathbf{s}_n)$ and its transpose $\mathbf{R}^{\intercal}$ obtained from $\mathbf{D}$, the 2PCFs data vector, and $\mathbf{T}(\mathbf{s}_{\rm c}, \mathbf{s}_n)$, their theory prediction for a given model described by the parameter sets $\mathbf{s}_{\rm c}$ and $\mathbf{s}_n$, and with Cov being their covariance matrix. We introduced two changes with respect to the DES Y3 work (Abbott et al. 2022). First, instead of the priors listed in Table I of Abbott et al. (2022), we imposed the above wider priors on Ω_m and H_0. Second, we used the NAUTILUS[3] (Lange 2023) nested sampler algorithm within the COSMOSIS[4] (Zuntz et al. 2015) software infrastructure.

[2] https://doi.org/10.5281/zenodo.16919645 (Version v1).

[3] Configuration: n_live=10000, n_networks=16.

[4] https://cosmosis.readthedocs.io/

For the standard siren analysis, we assumed a hierarchical Bayesian likelihood given by

$$\mathcal{L}\left(D_{\rm GW}\left|\mathbf{s}_{\rm c},\mathbf{s}_n\right.\right) \propto \prod_i^{N_{\rm det}} \frac{\int {\rm d}\boldsymbol{\theta}\, \mathcal{L}(D_{{\rm GW},i}|\boldsymbol{\theta})\, \pi(\boldsymbol{\theta}|\mathbf{s}_{\rm c},\mathbf{s}_n)}{\xi(\mathbf{s}_{\rm c},\mathbf{s}_n)}, \tag{2}$$

where $D_{\rm GW}$ is the ensemble of GW events data, $N_{\rm det}$ is the number of GW detections used in the analysis, $\mathcal{L}(D_{{\rm GW},i}|\boldsymbol{\theta})$ is the single-event GW likelihood given the intrinsic single-event parameters $\boldsymbol{\theta}$ describing the binary, $\pi(\boldsymbol{\theta}|\mathbf{s}_{\rm c},\mathbf{s}_n)$ is the population prior, and $\xi(\mathbf{s}_{\rm c},\mathbf{s}_n)$ is a term that represents the expected fraction of detected events in the population for a given set of cosmological and population parameters; this term accounts for GW selection effects. For the spectral siren analysis, we assumed the population model FULLPOP-4.0 (Fishbach et al. 2020; Farah et al. 2022; Mali & Essick 2025; Abac et al. 2025a), which includes a merger-rate model with redshift evolution (Madau & Dickinson 2014) and a mass model describing the neutron star and black hole mass ranges. We refer to Table 5 of Abac et al. (2025a) for the LVK priors. For the spectral sirens, we used the existing outputs of the official LVK analysis. For GW170817, we also reran the H_0 inference using the d_L posterior samples with added jet information. We performed our GW170817 re-analysis of H_0 with `gwcosmo` (Gray et al. 2020, 2022, 2023). The population prior was assumed to be a uniform distribution in mass ($[1, 3]\, M_\odot$) with merger-rate parameters fixed as in Abac et al. (2025a) and with a velocity relative to the Hubble flow $v_H = 3017 \pm 166\,{\rm km\,s^{-1}}$ obtained by subtracting the recession velocity and peculiar velocity of NGC 4993 (Abbott et al. 2017a). To facilitate combination later on, and noting that GW170817 is at a very low redshift ($\sim$0.01) and therefore is not sensitive to the Ω_m parameter, we augmented the bright siren H_0 samples by adding a prior-dominated sample within the uniform interval $\Omega_m \in [0, 1]$. We then combined the spectral and bright sirens posteriors to obtain the standard siren posterior distribution, which we next combined with the 3×2 pt posterior.

To evaluate the consistency of the posterior distributions from 3×2 pt and standard sirens, we computed the distance between the medians of the H_0 posteriors, expressed in units of the combined standard deviation. We found a distance of 0.78σ, indicating good agreement between the two distributions. For Ω_m, this requirement is automatically satisfied because neither spectral nor bright sirens place any significant constraints. After verifying that the consistency criterion was met, we proceeded with combining the posteriors.

We combined the posterior samples from the 3×2 pt and spectral sirens analyses using the normalising flow method presented in Gatti et al. (2025), Raveri et al. (2024), as implemented in `tensiometer`[5]. This approach assumes that the individual posteriors are not mutually in tension, and that the priors on common parameters, H_0 and $\Omega_{\rm m}$, are consistent.

4. Results

Figure 1 shows our combined measurement as well as the contributions of each major component. Table A.1 provides summary statistics including sub-components and alternative analysis choices. The 3×2 pt-only model yields a precision constraint of 17% on H_0, while the standard sirens reach 7%. When combined, the resulting precision is 6.4%, with $H_0 = 67.94^{+4.40}_{-4.34}\,{\rm km\,s^{-1}\,Mpc^{-1}}$ (median and 68% credible interval). When the jet properties of GW170817 are excluded from the analysis, the precision in H_0 decreases to 15% from standard sirens alone and to 9.9% after combination. The added constraining power of the 3×2 pt is 10–30% depending on whether the jet information is considered.

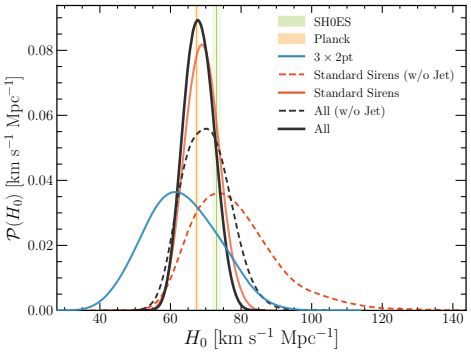

Fig. 1. Marginalised H_0 constraints from the 3×2 pt analysis (blue), the spectral sirens plus GW170817 analysis (red), and their combination (black). The results obtained excluding the jet information are also shown (dashed lines). The orange and green bands are CMB (Planck Collaboration VI 2020) and SNe Ia (Riess et al. 2022) constraints at the 68% credible interval.

Table A.1 shows that the contribution of GW170817 to the overall standard siren analysis is significantly dominant only when the jet information is included. This is consistent with the fact that the constraining power of GW170817 without inclination angle information and the spectral sirens is similar for this dataset (Abac et al. 2025a). The consistency between results with and without the jet information ($<1\sigma$) is also notable. This indicates that potential biases due to mismodelling of the jet or misalignment between the jet-inferred angle and the true plane of the binary (Müller et al. 2024) are subdominant.

Figure 2 shows our results in the H_0–Ω_m plane. Summary statistics for Ω_m are also provided in Table A.1. While the standard siren analysis presented here is not sensitive to Ω_m per se, its combination with 3×2 pt has a significant effect in this plane. We gauged the gain in constraining power due to 3×2 pt with the standard siren combination compared to the fiducial prior assumed in the DES Y3 analysis (Abbott et al. 2022), which is narrower in H_0 (flat range $[55, 91]\,{\rm km\,s^{-1}\,Mpc^{-1}}$) and Ω_m (flat range [0.1, 0.9]). The precision in H_0 derived from the 3×2 pt with narrower priors is 13% (see Table A.1). Therefore, in comparison to the fiducial DES Y3 analysis (with tighter priors driven by external experiments), the information injected from the combination with standard siren doubles the precision in H_0 measurement. Notably, the precision in the Ω_m measurement also benefits from the combination of 3×2 pt and standard sirens, improving from 11% to 8.2% (a relative improvement of 22%) compared to the DES fiducial priors.

5. Conclusions

In this Letter, we presented the first measurement of the Hubble constant from a combined probes analysis that integrates GW standard sirens in the 3×2 pt framework of joint weak-lensing and galaxy clustering analyses from cosmic surveys. We used the DES Y3 source and lens galaxy catalogues and 142 GW events from the LVK GWTC-4.0 catalogue: 141 spectral sirens, for which redshift information was derived from the mass distribution of its population, plus one bright siren, GW170817, which has a well-studied EM counterpart.

We measured $H_0 = 67.94^{+4.40}_{-4.34}\,{\rm km\,s^{-1}\,Mpc^{-1}}$ (6.4% precision). We further showed that a large fraction of the fiducial constraint comes from the jet information, with the precision

[5] https://tensiometer.readthedocs.io/

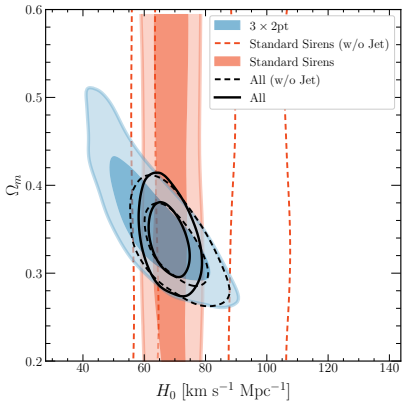

Fig. 2. Marginalised constraints on H_0 and Ω_m from the 3×2 pt (blue), the standard sirens (red), and the combination (black). The results obtained without the GW170817 jet information are also shown (dashed). The contours show 1σ and 2σ credible levels.

decreasing to 9.9% when this was removed. Relative to the standard siren analysis alone, the 3×2 pt combination yields an improvement of 10–30% on the H_0 uncertainties, depending on whether the jet information is used. We also assessed the effect of our joint analysis on Ω_m. While the standard siren component alone is uninformative over this parameter, the combination leads to an improvement of 22% in the Ω_m uncertainties relative to the DES Y3 3×2 pt result alone. This improvement demonstrates that standard sirens have sufficient constraining power to be informative when combined with 3×2 pt probes, similarly to what is done with CMB, SNe Ia, or baryon acoustic oscillations.

This result bodes well for future analyses using new data releases from DES and LVK in the near term as well as for the next generation of observatories in the long run. Full combined analyses, along the lines presented here, will leverage the combined constraining power of GW and 3×2 pt to reach a percent-level precision on H_0 and advance the field of cosmology at a faster pace than otherwise expected.

Acknowledgements. Funding for this work is provided by the University of Zurich (UZH) and the Swiss National Science Foundation (SNSF) under grant number 10002981. DL is supported by the UZH Postdoc Grant, grant no. [K-72341-01-01]. This material is based upon work supported by NSF's LIGO Laboratory which is a major facility fully funded by the National Science Foundation. This project used public archival data from the Dark Energy Survey (DES). Funding for the DES Projects has been provided by the DOE and NSF(USA), MEC/MICINN/MINECO(Spain), STFC(UK), HEFCE(UK). NCSA(UIUC), KICP(U. Chicago), CCAPP(Ohio State), MIFPA(Texas A&M), CNPQ, FAPERJ, FINEP (Brazil), DFG(Germany) and the DES Collaborating Institutions. Based in part on observations at Cerro Tololo Inter-American Observatory, NOIRLAB, which is operated by the Association of Universities for Research in Astronomy (AURA) under a cooperative agreement with the NSF.

References

Aasi, J., Abbott, B. P., Abbott, R., et al. 2015, Class. Quant. Grav., 32, 074001
Abac, A. G., Abouelfettouh, I., Acernese, F., et al. 2025a, ArXiv e-prints [arXiv:2509.04348]
Abac, A. G., Abouelfettouh, I., Acernese, F., et al. 2025b, ApJ, 995, L18
Abac, A. G., Abouelfettouh, I., Acernese, F., et al. 2025c, ArXiv e-prints [arXiv:2508.18081]
Abac, A. G., Abouelfettouh, I., Acernese, F., et al. 2025d, ArXiv e-prints [arXiv:2508.18082]
Abac, A. G., Abouelfettouh, I., Acernese, F., et al. 2025e, ArXiv e-prints [arXiv:2508.18083]
Abbott, B. P., Abbott, R., Abbott, T. D., et al. 2017a, Nature, 551, 85
Abbott, B. P., Abbott, R., Abbott, T. D., et al. 2017b, Phys. Rev. Lett., 119, 161101
Abbott, B. P., Abbott, R., Abbott, T. D., et al. 2017c, ApJ, 848, L12
Abbott, B. P., Abbott, R., Abbott, T. D., et al. 2019, Phys. Rev. X, 9, 031040
Abbott, B. P., Abbott, R., Abbott, T. D., et al. 2021, ApJ, 909, 218
Abbott, T. M. C., Aguena, M., Alarcon, A., et al. 2022, Phys. Rev. D, 105, 023520
Abbott, R., Abe, H., Acernese, F., et al. 2023, ApJ, 949, 76
Acernese, F., Agathos, M., Agatsuma, K., et al. 2015, Class. Quant. Grav., 32, 024001
Akutsu, T., Ando, M., Arai, K., et al. 2021, PTEP, 2021, 05A101
Amon, A., Gruen, D., Troxel, M. A., et al. 2022, Phys. Rev. D, 105, 023514
Blazek, J., MacCrann, N., Troxel, M. A., & Fang, X. 2019, Phys. Rev. D, 100, 103506
Bom, C. R., Alfradique, V., Palmese, A., et al. 2024, MNRAS, 535, 961
Camphuis, E., Quan, W., Balkenhol, L., et al. 2026, Phys. Rev. D., 113, 083504
Carrick, J., Turnbull, S. J., Lavaux, G., & Hudson, M. J. 2015, MNRAS, 450, 317
Casertano, S., Anand, G., Anderson, R. I., et al. 2025, ArXiv e-prints [arXiv:2510.23823]
Cawthon, R., Elvin-Poole, J., Porredon, A., et al. 2022, MNRAS, 513, 5517
Crook, A. C., Huchra, J. P., Martimbeau, N., et al. 2007, ApJ, 655, 790
de Matos, I. S., Dalang, C., Baker, T., et al. 2025, ArXiv e-prints [arXiv:2512.15380]
De Vicente, J., Sánchez, E., & Sevilla-Noarbe, I. 2016, MNRAS, 459, 3078
Di Valentino, E., & Brout, D. 2024, The Hubble Constant Tension (Springer)
Efstathiou, G., & Gratton, S. 2021, OJAp, 4, 8
Elvin-Poole, J., MacCrann, N., Everett, S., et al. 2023, MNRAS, 523, 3649
Essick, R., Coughlin, M. W., Zevin, M., et al. 2025, Phys. Rev. D, 112, 102001
Ezquiaga, J. M., & Holz, D. E. 2022, Phys. Rev. Lett., 129, 061102
Fang, X., Eifler, T., & Krause, E. 2020, MNRAS, 497, 2699
Farah, A. M., Fishbach, M., Essick, R., Holz, D. E., & Galaudage, S. 2022, ApJ, 931, 108
Finke, A., Foffa, S., Iacovelli, F., Maggiore, M., & Mancarella, M. 2021, JCAP, 08, 026
Fishbach, M., Essick, R., & Holz, D. E. 2020, ApJ, 899, L8
Flaugher, B., Diehl, H. T., Honscheid, K., et al. 2015, AJ, 150, 150
Friedrich, O., Andrade-Oliveira, F., Camacho, H., et al. 2021, MNRAS, 508, 3125
Gatti, M., Sheldon, E., Amon, A., et al. 2021, MNRAS, 504, 4312
Gatti, M., Campailla, G., Jeffrey, N., et al. 2025, Phys. Rev. D, 111, 063504
Giannini, G., Alarcon, A., Gatti, M., et al. 2024, MNRAS, 527, 2010
Gray, R., Hernandez, I. M., Qi, H., et al. 2020, Phys. Rev. D, 101, 122001
Gray, R., Messenger, C., & Veitch, J. 2022, MNRAS, 512, 1127
Gray, R., Beirnaert, F., Karathanasis, C., et al. 2023, JCAP, 12, 023
Heymans, C., Tröster, T., Asgari, M., et al. 2021, A&A, 646, A140
Holz, D. E., & Hughes, S. A. 2005, ApJ, 629, 15
Hotokezaka, K., Nakar, E., Gottlieb, O., et al. 2019, Nature Astron., 3, 940
Hou, Z., Aylor, K., Benson, B. A., et al. 2018, ApJ, 853, 3
Karathanasis, C., Mukherjee, S., & Mastrogiovanni, S. 2023, MNRAS, 523, 4539
Krause, E., & Eifler, T. 2017, MNRAS, 470, 2100
Krause, E., Fang, X., Pandey, S., et al. 2021, ArXiv e-prints [arXiv:2105.13548]
Lange, J. U. 2023, MNRAS, 525, 3181
Louis, T., La Posta, A., Atkins, Z., et al. 2025, JCAP, 11, 062
MacCrann, N., Becker, M. R., McCullough, J., et al. 2021, MNRAS, 509, 3371
Madau, P., & Dickinson, M. 2014, ARA&A, 52, 415
Mali, U., & Essick, R. 2025, ApJ, 980, 85
Mandel, I., Farr, W. M., & Gair, J. R. 2019, MNRAS, 486, 1086
Mastrogiovanni, S., Laghi, D., Gray, R., et al. 2023, Phys. Rev. D, 108, 042002
Miyatake, H., Sugiyama, S., Takada, M., et al. 2023, Phys. Rev. D, 108, 123517
Mooley, K. P., Deller, A. T., Gottlieb, O., et al. 2018, Nature, 561, 355
Mukherjee, S., Krolewski, A., Wandelt, B. D., & Silk, J. 2024, ApJ, 975, 189
Müller, M., Mukherjee, S., & Ryan, G. 2024, ApJ, 977, L45
Palmese, A., Bom, C. R., Mucesh, S., & Hartley, W. G. 2023, ApJ, 943, 56
Pandey, S., Krause, E., DeRose, J., et al. 2022, Phys. Rev. D, 106, 043520
Planck Collaboration VI. 2020, A&A, 641, A6
Porredon, A., Crocce, M., Fosalba, P., et al. 2021, Phys. Rev. D, 103, 043503
Porredon, A., Crocce, M., Elvin-Poole, J., et al. 2022, Phys. Rev. D, 106, 103530
Prat, J., Blazek, J., Sánchez, C., et al. 2022, Phys. Rev. D, 105, 083528
Raveri, M., Doux, C., & Pandey, S. 2024, Open Rev. [arXiv:2409.09101]
Riess, A. G., Yuan, W., Macri, L. M., et al. 2022, ApJ, 934, L7
Rodríguez-Monroy, M., Weaverdyck, N., Elvin-Poole, J., et al. 2022, MNRAS, 511, 2665
Secco, L. F., Samuroff, S., Krause, E., et al. 2022, Phys. Rev. D, 105, 023515
Sevilla-Noarbe, I., Bechtol, K., Carrasco Kind, M., et al. 2021, ApJS, 254, 24
Soares-Santos, M., Palmese, A., Hartley, W., et al. 2019, ApJ, 876, L7
Taylor, S. R., Gair, J. R., & Mandel, I. 2012, Phys. Rev. D, 85, 023535
Vitale, S., Gerosa, D., Farr, W. M., & Taylor, S. R. 2022, Hdbk. of Gravitational Wave Astronomy (Springer), 45
Wright, A. H., Stölzner, B., Asgari, M., et al. 2025, A&A, 703, A158
Zuntz, J., Paterno, M., Jennings, E., et al. 2015, Astron. Comput., 12, 45

Appendix A: Summary Statistics Table

Table A.1. H_0 and Ω_m measurements.

	H_0 [km s^{-1} Mpc^{-1}]	Ω_m
3×2pt	$62.80^{+11.49}_{-10.24}$ (60.02)	$0.352^{+0.055}_{-0.041}$
Standard Sirens (w/o Jet)	$76.45^{+13.12}_{-9.99}$ (76.78)	–
Standard Sirens	$68.95^{+4.75}_{-4.90}$ (68.21)	–
All (w/o Jet)	$70.16^{+6.82}_{-7.02}$ (69.10)	$0.331^{+0.031}_{-0.031}$
All	$67.94^{+4.40}_{-4.34}$ (67.89)	$0.338^{+0.028}_{-0.028}$
3×2pt (w/ DES priors)	$65.18^{+9.94}_{-6.90}$ (58.03)	$0.345^{+0.036}_{-0.036}$
GW170817 (w/o Jet)	$78.47^{+25.87}_{-11.98}$ (69.15)	–
GW170817	$68.77^{+4.94}_{-4.75}$ (68.58)	–

Notes. Values reported as the median and 68% credible interval of the posterior probability distribution, accompanied by maximum a posteriori (MAP) values in parenthesis. The top five rows correspond to the results shown in the figures. The bottom three rows are analysis variations shown for comparison.